Modulation of Excited State Property Based on Benzo[a, c]phenazine Acceptor: Three Typical Excited States and Electroluminescence Performance

Changjiang Zhou[1], Shengbing Xiao[1], Man Wang[1], Wenzhe Jiang[1], Haichao Liu[1], Shitong Zhang[1,2]* and Bing Yang[1]*

[1] *State Key Laboratory of Supramolecular Structure and Materials, College of Chemistry, Jilin University, Changchun, China,*
[2] *Institute of Theoretical Chemistry, Jilin University, Changchun, China*

Throwing light upon the structure-property relationship of the excited state properties for next-generation fluorescent materials is crucial for the organic light emitting diode (OLED) field. Herein, we designed and synthesized three donor-acceptor (D-A) structure compounds based on a strong spin orbit coupling (SOC) acceptor benzo[a, c]phenazine (DPPZ) to research on the three typical types of excited states, namely, the locally-excited (LE) dominated excited state (CZP-DPPZ), the hybridized local and charge-transfer (HLCT) state (TPA-DPPZ), and the charge-transfer (CT) dominated state with TADF characteristics (PXZ-DPPZ). A theoretical combined experimental research was adopted for the excited state properties and their regulation methods of the three compounds. Benefiting from the HLCT character, TPA-DPPZ achieves the best non-doped device performance with maximum brightness of 61,951 cd m^{-2} and maximum external quantum efficiency of 3.42%, with both high photoluminescence quantum efficiency of 40.2% and high exciton utilization of 42.8%. Additionally, for the doped OLED, PXZ-DPPZ can achieve a max EQE of 9.35%, due to a suppressed triplet quenching and an enhanced SOC.

Keywords: OLED, phenazine, donor-acceptor, spin-orbit coupling, hybridization state

INTRODUCTION

Over the past few decades, organic light-emitting diodes (OLEDs) have attracted much attention from academia to industry due to their advantages for high quality flat panel display and lighting applications (Tang and VanSlyke, 1987; Cao et al., 1999; Xiang et al., 2013; Jin et al., 2014; Yao et al., 2014; Krotkus et al., 2016; Chen et al., 2017, 2018; Liu et al., 2017a). For the cheap, metal-free pure organic fluorescent molecules, effective utilization of triplet exciton is the major issue to achieve high performance device according to the spin statistics rules in electro-excitons that are generated through the combination of hole- and electron-carriers (Atkins and Friedman, 2011; Lee et al., 2014; Chen et al., 2016; Guo F. et al., 2017). By now, three main mechanisms have been proposed to utilize the 75% electro-triplet excitons: the thermally-activated delayed fluorescence (TADF)(Uoyama et al., 2012; Zhang et al., 2014a,b; Zhang D. et al., 2015; Guo J. et al., 2017), the

triplet–triplet annihilation (TTA)(Luo and Aziz, 2010; Chiang et al., 2013) and the hybridized local and charge-transfer (HLCT) state(Li et al., 2012; Yao et al., 2015; Zhang S. et al., 2015; Wang et al., 2016, 2017; Tang et al., 2018). Recently, Li et al also reported a highly efficient near-infrared OLED utilizing doublet excited state, which is a promising method for 100% electro-exciton utilization (Peng et al., 2015; Ai et al., 2018a,b). Especially, the HLCT excited state is decent for fast triplet utilization and high photoluminescent (PL) efficiency, which is a promising method for the next-generation OLED materials. Generally, the excited states of pure organic material can be mainly divided into two kinds: the locally-excited (LE) state and the charge-transfer (CT) state (Gao et al., 2016; Zhou et al., 2018a). The LE state possesses large orbital overlap between the hole and electron wave functions, which usually possesses higher oscillator strength, corresponding to a larger radiative transition probability; while the CT state exhibits separated wave functions between hole and electron, and it is usually considered of non-emissive. However, the CT excited state is in favor of harvesting triplet excitons through a narrowed energy splitting between singlet and triplet states. Thus, the HLCT excited state contains a coexistence of LE and CT characters, and simultaneous high PL efficiency with high exciton utilization in OLED is expected to achieve through rational state regulation(Li et al., 2014b; Liu et al., 2015, 2017b; Zhou et al., 2017).

The explanation of high electro-triplet utilization of HLCT excited state is currently explained as going through a "hot-exciton" channel(Li et al., 2014a; Pan et al., 2014), but the essential mechanism is still under researching. Generally, the triplet utilization relies on the reversed intersystem crossing (RISC) process. Inspiring by the works on the room-temperature phosphorescence (RTP) materials, enhancing the spin-orbit coupling (SOC) can be a decent method to further accelerate the RISC for triplet utilization(Mao et al., 2015; Xu et al., 2016; Liu et al., 2018; Sun et al., 2018). Recently we have reported a singles-molecular white emissive material benzo[a, c]phenazine (DPPZ), which can realize a ternary emission of T_2-RTP, T_1-RTP, and S_1-RTP (**Figure 1**) (Zhou et al., 2018b). We have proved that the two sp^2-hybridized nitrogen atoms greatly contribute to the enhanced SOC in DPPZ ($\sim 10 \, cm^{-1}$) according to the El-Sayed rule(El-Sayed, 1963, 1964), and obviously, for the same reason, it can also be a suitable acceptor for the donor-acceptor (D-A) material, which is expectable for realizing decent electroluminescent (EL) performances. However, the sp^2-hybridized nitrogen atom also causes problem in efficient emission, since the n→ π^* transition always performance badly in oscillator strength. Therefore, to overcome this problem, rational remolding of the excited state of DPPZ is necessary. In our previous work, introducing a proper CT excited state component to build up a HLCT excited state is an effective solution. Considering the energy-level arrangement of LE and CT origin excited states, three kinds of possible energy structures could be concluded between LE and CT states: (1) low-lying LE and high-lying CT, (2) LE lies close to CT, and (3) high-lying LE and low-lying CT (**Scheme 1**). Obviously, (1) and (3) are not desired model for DPPZ derivates, since the LE (originate from DPPZ) and the CT (Donor moiety → DPPZ)

are neither emissive. Judging from the state-mixing principle (Equation 1 and 2):

$$\psi\,(S_1) = \psi\,(LE) + \lambda \times \psi\,(CT) \tag{1}$$

$$\lambda = \left| \frac{\langle \psi_{LE} \,|H|\, \psi_{CT} \rangle}{E_{LE} - E_{CT}} \right| \tag{2}$$

where λ is the mixing coefficient that represents the degree of hybridization between LE and CT, and λ is mainly determined by two factors: the energy gap of the non-adiabatic LE and CT states $E_{LE} - E_{CT}$, and the magnitude of their interstate coupling $\langle \psi_{LE} \,|H|\, \psi_{CT} \rangle$. Obviously, it is easier to regulate $E_{LE} - E_{CT}$ by choosing different donor units, and at the same time, its essential structure-property relationship can be further understood.

In this work, based on the DPPZ acceptor, we designed and synthesized three D-A compounds with three typical donor moieties (CZP, phenyl-carbarzole; TPA, triphenylamine; PXZ, phenoxazine), which corresponds to three typical excited states characteristics: the LE-dominated excited state (CZP-DPPZ), the HLCT (TPA-DPPZ) and CT state with TADF characters (PXZ-DPPZ). Among these three molecules, the HLCT material TPA-DPPZ obtains both high quantum efficiency of 40.2% and high exciton utilization of 42.8% in the non-doped OLED, benefiting from the HLCT character that arises the radiative transition rate and restrains the non-radiative transition, and eventually achieves the best non-doped OLED performance among the three materials with a maximum external quantum efficiency (EQE) of 3.42%. Additionally, The TADF material PXZ-DPPZ also demonstrates an efficient orange-red electro-fluorescence in doped OLED with an EQE of 9.35%.

MATERIALS AND METHODS

Synthesis

All the reagents and solvents used for the synthesis were purchased from Aldrich or Acros and used as received. All reactions were performed under nitrogen atmosphere. The synthesis of precursor reactants can be found in our previous work.

11-bromodibenzo[a, c]phenazine

A mixture of phenanthrene-9,10-dione (5 mmol) and 4-bromobenzene-1,2-diamine (5 mmol) in acetic acid (80 mL) was heated to reflux for 8 h. After cooling to room temperature, the resulting mixture was poured into ethanol (200 mL), and then filtered. The solid was washed with ethanol several times. The crude product was purified by column chromatography on silica gel (eluent: dichloromethane) and dried under vacuum to give the desired compound as a yellow solid in 90% yield (1.62 g). ^{1}H NMR (500 MHz, CDCl$_3$): δ 9.46–9.32 (m, 2H), 8.59 (d, J = 8.1 Hz, 2H), 8.56 (d, J = 2.0 Hz, 1H), 8.23 (d, J = 9.0 Hz, 1H), 7.94 (dd, J = 9.0, 2.1 Hz, 1H), 7.84 (t, J = 7.5 Hz, 2H), 7.78 (t, J = 7.5 Hz, 2H). MALDI-TOF MS (mass m/z): 361.4 [M(H)] $^+$.
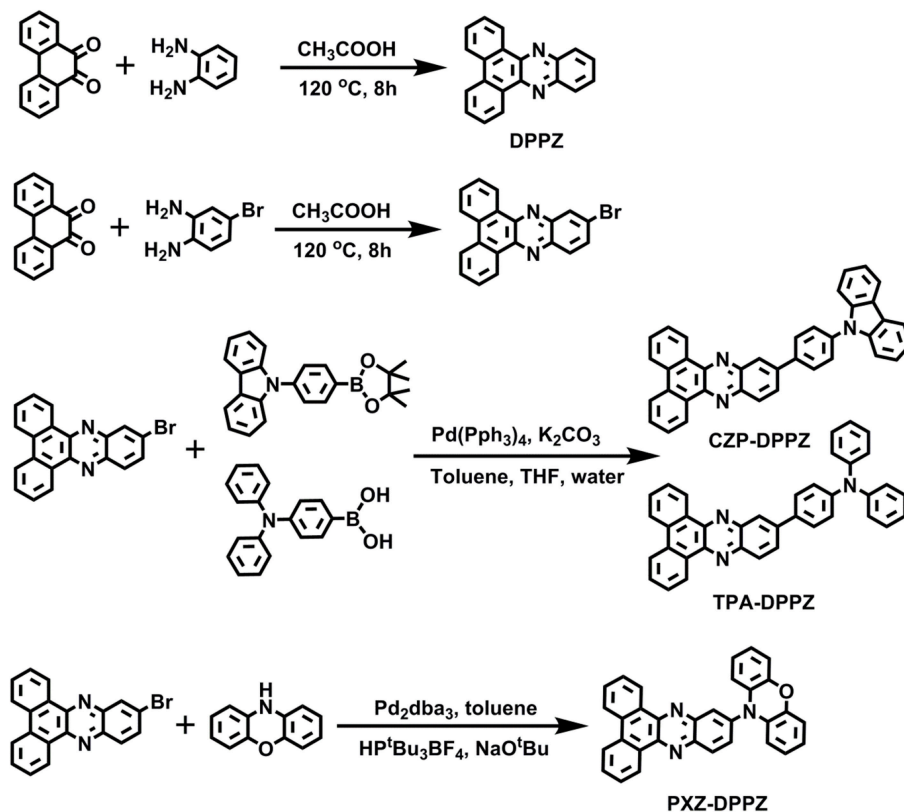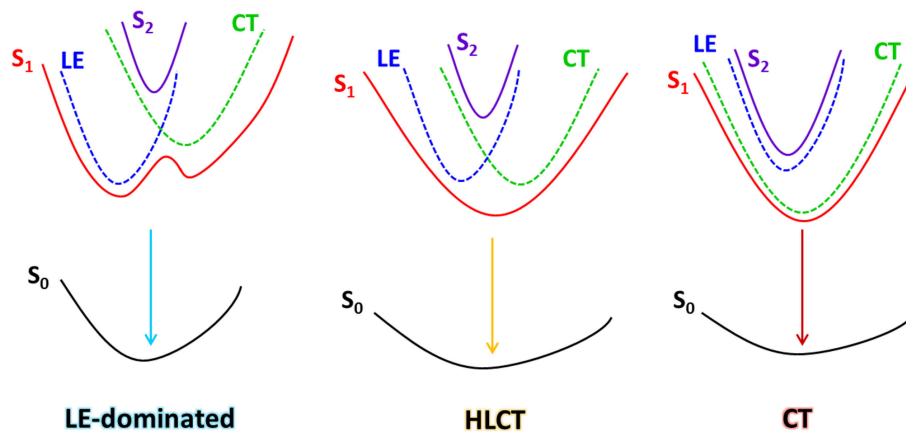
FIGURE 1 | The chemical equations for the synthesis of DPPZ, CZP-DPPZ, TPA-DPPZ, and PXZ-DPPZ.

SCHEME 1 | Schematic diagram of interaction between LE and CT excited states.

11-(4-(9H-carbazol-9-yl)phenyl)dibenzo[a, c] phenazine (CZP-DPPZ)

A mixture of 9-(4-(4,4,5,5-tetramethyl-1,3,2-dioxaborolan-2-yl)phenyl)-9H-carbazole (2.6 mmol) (Wang et al., 2016), 11-bromodibenzo[a, c]phenazine (2.0 mmol), sodium carbonate (20 mmol), toluene (15 mL), absolute alcohol (10 ml) and deionized water (10 mL), with $Pd(PPh_3)_4$ (60 mg) acting as catalyst was

refluxed at 90°C for 48 h under nitrogen. After the mixture was cooled down, 40 mL water was added to the resulting solution and the mixture was extracted with CH_2Cl_2 for several times. The organic phase was dried over Na_2SO_4. After filtration and solvent evaporation, the liquid was purified by chromatography using the mixture of CH_2Cl_2/petroleum ether as the eluent to afford a pale green solid in 75% yield (0.78 g). ^{1}H NMR (500 MHz, $CDCl_3$):

δ 9.59 (d, $J = 7.9$ Hz, 1H), 9.53 (d, $J = 7.6$ Hz, 1H), 8.84 (s, 1H), 8.64 (d, $J = 7.6$ Hz, 2H), 8.58 (d, $J = 8.8$ Hz, 1H), 8.30 (dd, $J = 8.8$, 1.6 Hz, 1H), 8.21 (d, $J = 7.8$ Hz, 2H), 8.15 (d, $J = 8.3$ Hz, 2H), 7.86 (ddd, $J = 22.6$, 14.0, 7.6 Hz, 6H), 7.58 (d, $J = 8.2$ Hz, 2H), 7.50 (t, $J = 7.3$ Hz, 2H), 7.36 (t, $J = 7.4$ Hz, 2H). MALDI-TOF MS (mass m/z): 522.7 [M(H)]$^+$. Anal. calcd for $C_{38}H_{23}N_3$: C 87.50, H 4.44, N 8.06; found: C 87.13, H 4.68, N 8.16.

4-(dibenzo[a, c]phenazin-11-yl)-N,N-diphenylaniline (TPA-DPPZ)

A mixture of N,N-diphenyl-4-(4,4,5,5-tetramethyl-1,3,2-dioxaborolan-2-yl)aniline (2.6 mmol), 11-bromodibenzo[a, c]phenazine (2.0 mmol), sodium carbonate (20 mmol), toluene (15 mL), absolute alcohol (10 ml) and deionized water (10 mL), with Pd(PPh₃)₄ (60 mg) acting as catalyst was refluxed at 90°C for 48 h under nitrogen. After the mixture was cooled down, 40 mL water was added to the resulting solution and the mixture was extracted with CH_2Cl_2 for several times. The organic phase was dried over Na_2SO_4. After filtration and solvent evaporation, the liquid was purified by chromatography using the mixture of CH_2Cl_2/petroleum ether as the eluent to afford a yellow-green solid in 75% yield (0.78 g). ^{1}H NMR (500 MHz, CDCl₃): δ 9.59 (d, $J = 7.8$ Hz, 1H), 9.49 (d, $J = 6.9$ Hz, 1H), 8.73 (s, 1H), 8.62 (dd, $J = 7.8$, 3.7 Hz, 2H), 8.48 (d, $J = 8.8$ Hz, 1H), 8.21 (dd, $J = 8.9$, 1.9 Hz, 1H), 7.92–7.74 (m, 6H), 7.40–7.32 (m, 4H), 7.27–7.18 (m, 6H), 7.12 (t, $J = 7.4$ Hz, 2H). MALDI-TOF MS (mass m/z): 524.2 [M(H)]$^+$. Anal. calcd for $C_{38}H_{25}N_3$: C 87.16, H 4.81, N 8.02; found: C 86.92, H 4.75, N 8.32.

10-(dibenzo[a, c]phenazin-11-yl)-10H-phenoxazine (PXZ-DPPZ)

A mixture of 10H-phenoxazine (2.0 mmol), 11-bromodibenzo[a, c]phenazine (2.2 mmol), HPtBu₃BF₄ (0.1 mmol), Sodium tert-butoxide (2.3 mmol), toluene (10 mL), with Pd₂(dba)₃ (0.06

mmol) acting as catalyst was refluxed at 110°C for 48 h under nitrogen. After the mixture was cooled down, 40 mL water was added to the resulting solution and the mixture was extracted with CH_2Cl_2 for several times. The organic phase was dried over Na_2SO_4. After filtration and solvent evaporation, the liquid was purified by chromatography using the mixture of CH_2Cl_2/petroleum ether as the eluent to afford a red solid in 60% yield (0.55 g). ^{1}H NMR (500 MHz, CDCl₃): δ 9.47 (dd, $J = 8.0$, 1.1 Hz, 1H), 9.44 (dd, $J = 8.0$, 1.0 Hz, 1H), 8.60 (dd, $J = 14.0$, 8.5 Hz, 3H), 8.48 (d, $J = 2.2$ Hz, 1H), 7.94–7.72 (m, 5H), 6.81 (dd,
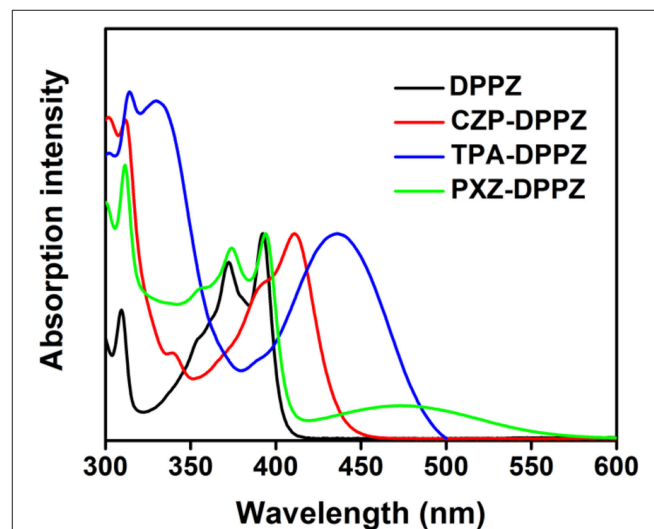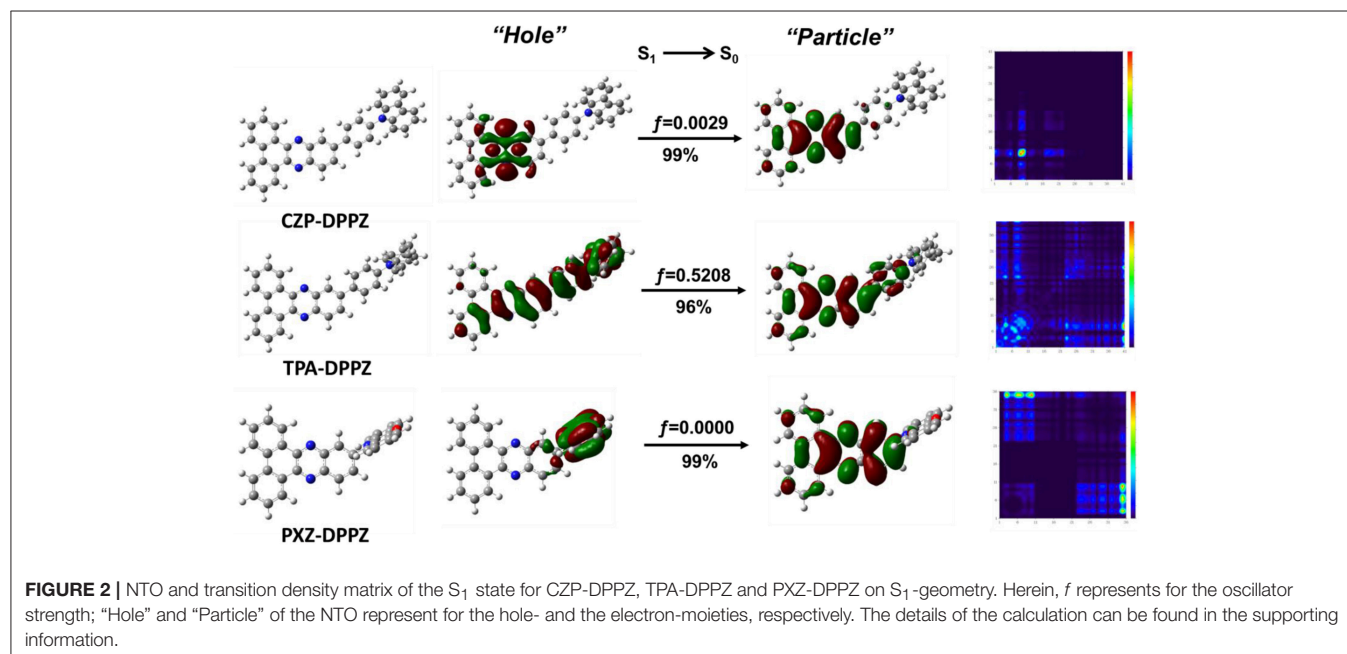

FIGURE 3 | The UV-vis spectra of DPPZ and three D-A structure molecules in THF solution (the concentration is 1×10^{-5} mol L^{-1}).

FIGURE 2 | NTO and transition density matrix of the S$_1$ state for CZP-DPPZ, TPA-DPPZ and PXZ-DPPZ on S$_1$-geometry. Herein, f represents for the oscillator strength; "Hole" and "Particle" of the NTO represent for the hole- and the electron-moieties, respectively. The details of the calculation can be found in the supporting information.

$J = 7.9$, 1.5 Hz, 2H), 6.75 (td, $J = 7.7$, 1.4 Hz, 2H), 6.66 (td, $J = 7.7$, 1.5 Hz, 2H), 6.20 (dd, $J = 8.0$, 1.3 Hz, 2H). MALDI-TOF MS (mass m/z): 462.8 $[M(H)]^+$. Anal. calcd for $C_{32}H_{19}N_3O$: C 83.28, H 4.15, N 9.10, O 3.47; found: C 83.02, H 4.41, N 9.22, O 3.24.

RESULTS AND DISCUSSION

Molecular Design

Structures

The structures of the compounds are illustrated in **Figure 1**. To gain a primary understanding of these compounds, we carried out the geometrical optimization and calculated their frontier orbital distributions (the highest occupied molecular orbital, HOMO; the lowest unoccupied molecular orbital, LUMO; in **Figure S1**) (Zhao and Truhlar, 2008; Frisch et al., 2009). The three compounds are all of separated HOMO and LUMO, in which the HOMOs locate on the donor moieties, whereas the LUMOs distribute on DPPZ. This bipolar molecule character is

beneficial for the balanced carrier transport in OLED. Notably, the twist angle between donor and acceptor for PXZ-DPPZ is as large as 78° due to the large steric hindrance, while the dihedral angles for the other two compounds are around 35° (**Table S1**). Such an orthogonal molecular conformation may largely break the conjugation between PXZ and DPPZ, leading to a strong CT transition of its emissive excited state. The HOMO energy level of CZP-DPPZ, TPA-DPPZ and PXZ-DPPZ are measured as −5.58 eV, −5.26 eV, and −5.09 eV, respectively, which also implies that PXZ-DPPZ may possess an obvious CT character, while CZP-DPPZ can be a LE-like material.

Electron Transition Properties

To better understand the nature and character of excited states, we optimized the excited state geometries and calculated the natural transition orbital (NTO) of the emissive singlet state ($S_1 \rightarrow S_0$) for these compounds. As shown in **Figure 2**, the NTO "hole" and "particle" of CZP-DPPZ both localize on the DPPZ
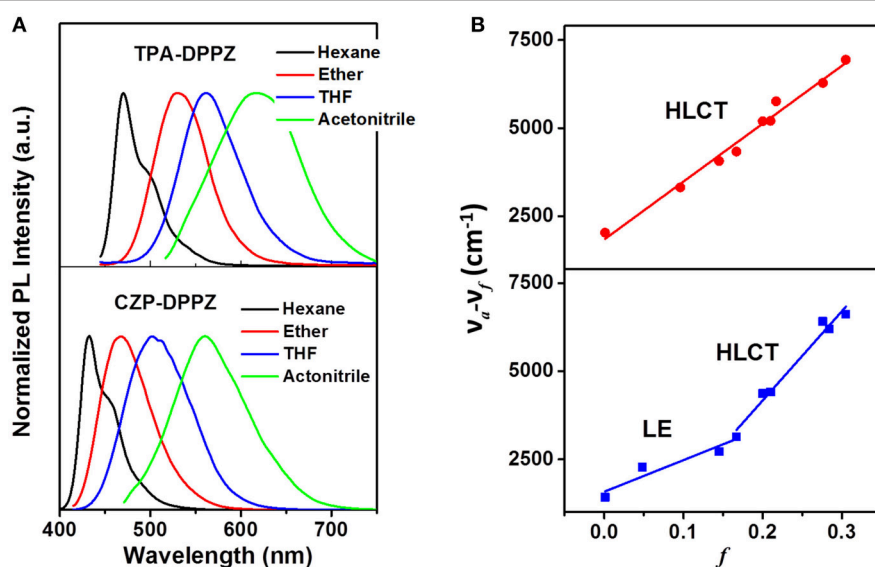

FIGURE 4 | (A) Solvent effect on the PL spectra of CZP-DPPZ, TPA-DPPZ and PXZ-DPPZ, in which the polarity f of the four solvents are $f_{hexane} = 0.0012$, $f_{ether} = 0.167$, $f_{THF} = 0.210$ and $f_{acetonitrile} = 0.305$. **(B)** Refined Lippert-Mataga model of CZP-DPPZ, TPA-DPPZ, and PXZ-DPPZ between Stokes shift and solvent polarity in more solvents. The details of the building of Lippert-Mataga model are in **Table S2**.
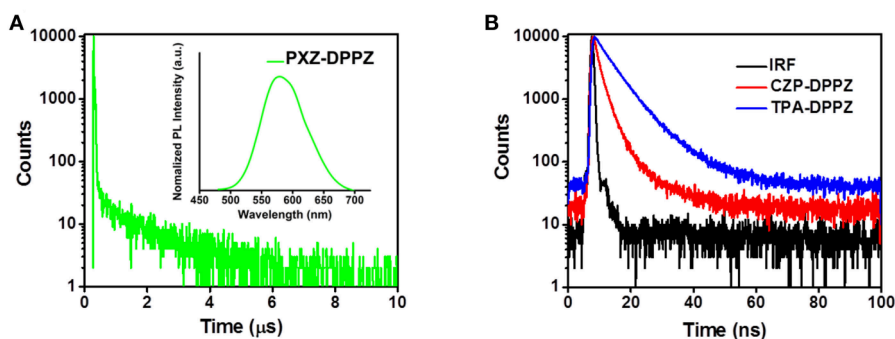

FIGURE 5 | (A) Lifetime and PL spectra of PXZ-DPPZ and **(B)** lifetimes of CZP-DPPZ and TPA-DPPZ in doped film.

moiety, which is almost the same to NTO of pure DPPZ (**Figure S2**). The oscillator strength of the S_1 state of CZP-DPPZ is 0.0029, which is only a little increasing comparing to that of DPPZ (0.0011), revealing that although certain state hybridization may occur, the S_1 state of CZP-DPPZ mainly exhibits an obvious LE character of $n \rightarrow \pi^*$ transition, which can result in a quenched fluorescence. On the other hand, the S_1 state of PXZ-DPPZ shows totally vertical, separated "hole" and "particle," assigning to an obvious CT character. And just for this reason, the oscillator strength of the S_1 excited state is calculated to be zero, which indicates that the radiative transition in DPPZ can be very poor. Additionally, the ΔE_{ST} (E_{S1}-E_{T1}) of PXZ-DPPZ is estimated as 0.0238 eV, suggesting that the strong donor PXZ can potentially contribute to TADF property for PXZ-DPPZ. Therefore, neither LE-dominated nor CT-dominated is a good state regulation method of DPPZ in enhancing its emission.

Different from the nearly absolute overlap (LE) or separated (CT) character, For the S_1 state of TPA-DPPZ, its "hole" and "particle" are partially overlapped, that is, LE and CT characters simultaneously exists in the S_1 excited state, according with the HLCT state character. Thanks to this efficient state hybridization, the oscillator strength of TPA-DPPZ S_1 excited state grows up to 0.5208, which is 170 times that of the LE-dominated CZP-DPPZ, indicating that TPA-DPPZ can be an emissive material by HLCT modulation. Additionally, the LE and CT compositions of the three materials can be quantitatively estimated using the transition density matrix method (Gao et al., 2016) (**Figure S3**) to verify our judge on the excited state categories. The LE: CT proportions of the S_1 excited states of CZP-DPPZ, TPA-DPPZ and PXZ-DPPZ are 0.97:0.3, 0.49:0.51 and 0.13:0.87, respectively, which agrees well with their excited state properties of LE-dominated, HLCT and CT-dominated.

Photophysical Properties

The UV spectra of these compounds were recorded in tetrahydrofuran (THF) solution (**Figure 3**) in reference to that of the acceptor unit DPPZ. The DPPZ unit shows vibronic fine absorption with peaks at 371 nm and 391 nm, which is a typical character for the rigid condensed ring structure. Upon substitution of different donor moieties, characteristic absorptions can be observed to judge the excited state essences that we have predicted in the theoretical calculations. First, a single broadened absorption peak at 436 nm is observed in TPA-DPPZ, owning to the well hybridization of LE and CT. In the case of the strongest donor moiety, PXZ-DPPZ shows a new

absorption with onset of 570 nm, and the original absorption peak of DPPZ is fully reserved. The newly generated, weak absorption is of a small molar absorption coefficient of below 1,000 L mol^{-1} cm^{-1} which should be ascribed to a forbidden electron transition for the small orbital overlap and large twist angle, indicating a CT-dominate absorption character, reflecting that the LE and CT components are independent, or a de-hybridized LE and CT excited state components in PXZ-DPPZ. Surprisingly, the LE-like CZP-DPPZ does not display an overlapped absorption as DPPZ or PXZ-DPPZ, instead a red-shifted spectrum with a residual fine structure is observed, which indicates that its S_1 state is still mainly of LE state transition character of DPPZ, but certain state-hybridization of LE and CT has taken place, which may also affect its OLED performance.

The solvatochromic PL measurements are then conducted for further confirm the different excited state formation of these compounds. First, CZP-DPPZ and TPA-DPPZ both exhibit red-shifted emissions in the polarity-increasing solvents, assigning to CT character (**Figure 4**). In their refined Lippert-Mataga model (**Table S2**) (Grabowski et al., 2003), obviously, CZP-DPPZ shows a two-section line with two slopes, demonstrating a non-equivalent hybridization state with two different characters of excited state, which is in accordance to its absorption: though very little, certain CT component is actually hybridized into the emissive excited state of CZP-DPPZ. The dipole moment (μ_e) of CZP-DPPZ can be estimated to 13.57 D in low-polarity solvents and 22.74 D in high-polarity solvents, which could be assigned to a set of independent LE state and HLCT state, respectively. Different from CZP-DPPZ, in TPA-DPPZ, a good linear relation of the polarity factor f and the Stokes shift in all solvents is observed, corresponding to an undistinguished dipole moment of 18.41 D, assigning to the quasi-equivalent hybridization between LE and CT states. Besides, the single exponential lifetimes of TPA-DPPZ in different solvents are also

TABLE 1 | Photoluminescence quantum yields (PLQYs) of compounds in different states.

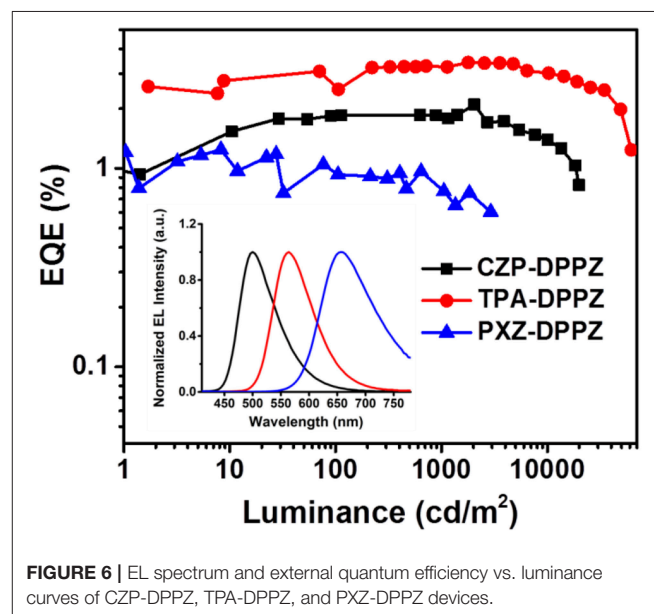| PLQY	CZP-DPPZ (%)	TPA-DPPZ (%)	PXZ-DPPZ (%)
Hexane	12	51	12
Ether	36	97	–
THF	81	93	–
Doped film	31	91	22
Powder	23	40	11

FIGURE 6 | EL spectrum and external quantum efficiency vs. luminance curves of CZP-DPPZ, TPA-DPPZ, and PXZ-DPPZ devices.

evidence that the excited state is one hybridized state (**Figure S4**), not a simple mix of two excited states (**Table S3**).

The "pure" CT compound PXZ-DPPZ demonstrates quite different PL compared to the other two compounds. We can only observe a very weak fluorescence in the lowest polarity solvent hexane with a PL peak at 566 nm (**Figure S5**), which is quite a red-shifted emission comparing to those of CZP-DPPZ and TPA-DPPZ, due to its obvious CT character caused by state de-hybridization. However, in higher-polarity solvents, the even strengthened CT character of PZX-DPPZ causes totally non-emissive, so that its Lippert-Mataga model cannot be built. In order to figure out its PL properties, we prepared a 5% doped film (w/w, PXZ-DPPZ in PMMA,) on neat quartz plate. As shown in **Figure 5A**, the doped film of PXZ-DPPZ shows an orange emission with a PL peak at 579 nm. Different from the other two compounds (**Figure 5B**), the CT compound PXZ-DPPZ demonstrates a typical TADF character, whose PL decay spectrum can be fitted as a bi-exponential model, where the delayed component (τ_d) exhibits a longer lifetime of 1.3 μs in the time range of 10 μs at room temperature, and the prompt component (τ_p) is estimated as 10.0 ns in the time range of 200 ns (**Figure S6**). Owning to the joint action of strong donor and orthogonal configuration, PXZ-DPPZ demonstrates a nearly zero overlap of wave functions, resulting in the small ΔE_{ST} and strong CT with TADF characters.

In addition, the photoluminescent quantum yield (PLQY) of three compounds are measured for different statuses (Solutions, doped films, and neat powder) in **Table 1**. As a result, the HLCT compound TPA-DPPZ keeps the highest quantum yields than others in any status, suggesting that the HLCT compound TPA-DPPZ is more promising than CZP-DPPZ and PXZ-DPPZ in non-doped OLED. Furthermore, the radiative and non-radiative transition rate constants of the three compounds are given out by theoretical calculation (**Table S4**) using the Molecular Materials Property Prediction Package (MOMAP) to understand the PLQY variation of the compounds (Peng et al., 2007, 2013). CZP-DPPZ displays a low radiative transition rate of 7.32×10^6 s^{-1}, which

originate from the non-emissive n→ π* character of LE state. Similarly, owing to the forbidden transition of CT state, PXZ-DPPZ exhibits the lowest k_r of 1.82×10^3 s^{-1} and corresponding to a low PLQY. But in the case of the HLCT material TPA-DPPZ, the k_r largely increases to 1.23×10^8 s^{-1}, more importantly, its k_{nr} also shows a significant suppression comparing to the LE compound CZP-DPPZ, which is in accordance to our previous work (Zhang et al., 2013).

Additionally, the seemingly non-emissive pure-CT compound PXZ-DPPZ is actually of considerable PLQY (11%). Although hard evidence has not been found yet, this phenomenon can be tentatively understood that the nuclear motion, such as the vibration and the rotation of D-A connection bond, i.e., electron-vibrational coupling (EVC) is expected to affect the emission of pure CT excited state in solid state (Chen et al., 2015; Etherington et al., 2016), which could be the basis that the TADF doped OLED is always highly efficient.

Electroluminescence Performances

The energy levels of the frontier orbital measured by cyclic voltammetry (CV) method for the three materials are listed in **Table S5**. The thermal gravimetric analysis (TGA) measurements are also carried out to examine their thermal stabilities. All the three compounds exhibit good thermal stability with thermal-decomposition temperature (T_d) over 430°C (**Figure S7**). The good thermal performance of these emissive materials will benefit the device stability in OLED.

The non-doped OLED using the three compounds as emitters are fabricated with typical multi-layer structure: indium tin oxide (ITO)/ hexaazatriphenylenehexacabonitrile (HATCN) (5 nm)/ 1,1′-bis(di-4-tolyl- aminophenyl)cyclohexane (TAPC)   (40 nm)/4,4′,4″-tri(N-carbazolyl)-triphenylamine (TCTA) (10 nm)/ emitter layer (20 nm)/ 1, 3, 5-tri(phenyl-2-benzimidazolyl)-benzene (TPBi) (40 nm)/ LiF (1 nm)/ Al (100 nm). Considering that the HOMO energy level of CZP is too deep (-5.58 eV), we add 4,4′-Bis(9H-carbazol-9-yl) biphenyl (CBP, HOMO = −5.91 eV) between TCTA and CZP-DPPZ as an

TABLE 2 | The electroluminescence device performances of emissive materials.

Emitter layer	V_{on} (V)[a]	λ_{max} (nm)[b]	L_{max} (cd m^{-2})[c]	$\eta_{LE/max}$(cd A^{-1})[d]	$\eta_{PE/max}$ (lm w^{-1})[e]	$\eta_{EQE/max}$(%)[f]	η_s (%)[g]
CZP-DPPZ	3.9	502	19,860	6.22	3.43	2.10	45.8
TPA-DPPZ	3.0	568	61,951	11.05	8.18	3.42	42.8
PXZ-DPPZ	3.6	656	2,918	0.61	0.52	1.24	49.0

[a]Turn-on voltage at a luminance of 1 cd m^{-2}; [b] Maximum peak of EL spectra; [c]maximum luminance; [d]Maximum luminous efficiency; [e] Maximum power efficiency; [f] maximum external quantum efficiency; [g]Electro-excition utilization.

TABLE 3 | Doped device performances of CZP-DPPZ, TPA-DPPZ, and PXZ-DPPZ.

Emitter layer	doping (wt%)	V_{on}(V)	λ_{max} (nm)	L_{max}(cd m^{-2})	$\eta_{LE/max}$ (cd A^{-1})	$\eta_{PE/max}$(lm w^{-1})	$\eta_{EQE/max}$ (%)
CZP-DPPZ	40	3.8	492	14,030	3.59	2.38	1.46
TPA-DPPZ	10	3.6	532	15,740	12.74	10.07	3.73
PXZ-DPPZ	5	3.6	616	10,430	14.30	11.49	9.35

The device structure is: HATCN(5 nm)/TAPA(30 nm)/TCTA(10 nm)/CBP: emitter(wt%)(20 nm)/TPBi(30 nm) /LiF(1nm)/Al(100 nm).

electron-blocking layer to avoid the formation of exciplex. The device performances are summarized in **Figure 6** and **Table 2**. The device based on CZP-DPPZ exhibits a green emission with a peak at 502 nm, and device of PXZ-DPPZ displays a red emission peaking at 656 nm (**Figure S8**), corresponding to the maximum external quantum efficiency (EQE) of 2.10 and 1.24%, respectively. Comparing to them, TPA-DPPZ based OLED shows significantly improved electroluminescence performance. It exhibits a lower turn-on voltage of 3.0 V, a larger maximum brightness of 61,951 cd m^{-2}, reflecting quite excellent stability of device (**Figure S10**). What's more, it achieves a max EQE of 3.42%, which 1.5 times that of CZP-DPPZ and 3 times that of PXZ-DPPZ. This efficiency increase can be assigned to the PLQY increasing brought about by HLCT, since the electro-exciton utilization of the three materials are just similar to each other, which is the result that the three compounds are all of certain CT excited state character (**Figure S9**), and non-negligibly, the strong SOC between singlet and triplet from DPPZ can also be a possible structural reason in parallel comparison to the acridine based D-A compounds that we have reported before (Zhou et al., 2017, 2018a).

The last but not the least, in previous works, the HLCT materials perform well in the non-doped OLED but the TADF materials do well in the doped OLED, although the k_r of TADF materials can be very limited. To investigate this issue, we also fabricated the doped OLED for these compounds, and the data are summarized in **Table 3**. Although the EQE of LE-dominated compound CZP-DPPZ and the HLCT compound TPA-DPPZ are kept as the same level as their non-doped OLED, the TADF material PXZ-DPPZ demonstrates an efficient orange-red emission with an 8-fold EQE (9.35%) that of its non-doped OLED (**Figure S11**), benefiting from its greatly suppressed triplet quenching and the probably existed EVC interaction that can drive the pure CT excited state be emissive.

CONCLUSIONS

In this work, to make the best use of the large SOC acceptor DPPZ, we synthesized three D-A compounds, which represent three typical excited states in fluorescent OLED: LE-dominated (CZP-DPPZ), HLCT (TPA-DPPZ), and CT (PXZ-DPPZ), and discussed the relationships between the structure and excited-state properties. Among them, the HLCT material TPA-DPPZ merits the highest k_r that is assigned to its enhanced oscillator

strength. As a result, TPA-DPPZ performs better than the other two materials in the non-doped OLED. For the doped OLED, despite its limited k_r, PXZ-DPPZ demonstrates a maximum EQE of 9.35%, which benefits from the greatly suppressed triplet quenching, high SOC originated from DPPZ acceptor and probably existed EVC. This work further proves that the regulation of HLCT excited state can be a decent method to design highly efficient organic functional materials, and also provides a new understanding to the structure-property relationship in fluorescent OLED.

DATA AVAILABILITY

All datasets generated for this study are included in the manuscript and/or the **Supplementary Files**.

AUTHOR CONTRIBUTIONS

FUNDING

ACKNOWLEDGMENTS

SUPPLEMENTARY MATERIAL

The Supplementary Material for this article can be found online at: https://www.frontiersin.org/articles/10.3389/fchem. 2019.00141/full#supplementary-material

REFERENCES

Ai, X., Chen, Y., Feng, Y., and Li, F. (2018a). A stable room-temperature luminescent biphenylmethyl radical. *Angew. Chem. Int. Ed.* 57, 2869–2873. doi: 10.1002/anie.201713321

Ai, X., Evans, E. W., Dong, S., Gillett, A. J., Guo, H., Chen, Y., et al. (2018b). Efficient radical-based light-emitting diodes with doublet emission. *Nature* 563, 536–540. doi: 10.1038/s41586-018-0695-9

Atkins, P. W., and Friedman, R. S. (2011). *Molecular Quantum Mechanics.* London: Oxford University Press.

Cao, Y., Parker, I. D., Yu, G., Zhang, C., and Heeger, A. J. (1999). Improved quantum efficiency for electroluminescence in semiconducting polymers. *Nature* 397, 414–417. doi: 10.1038/17087

Chen, H.-W., Lee, J.-H., Lin, B.-Y., Chen, S., and Wu, S.-T. (2018). Liquid crystal display and organic light-emitting diode display: present status and future perspectives. *Light Sci. Appl.* 7:17168. doi: 10.1038/lsa.2017.168

Chen, X.-K., Zhang, S.-F., Fan, J.-X., and Ren, A.-M. (2015). Nature of highly efficient thermally activated delayed fluorescence in organic light-emitting diode emitters: nonadiabatic effect between excited states. *J. Phys. Chem. C* 119, 9728–9733. doi: 10.1021/acs.jpcc.5b00276

Chen, Y.-H., Ma, D.-G., Sun, H.-D., Chen, J.-S., Guo, Q.-X., Wang, Q., et al. (2016). Organic semiconductor heterojunctions: electrode-independent charge injectors for high-performance organic light-emitting diodes. *Light Sci. Appl.* 5:e16042. doi: 10.1038/lsa.2016.42

Chen, Z., Zhang, C., Jiang, X.-F., Liu, M., Xia, R., Shi, T., et al. (2017). High-performance color-tunable perovskite light emitting devices through structural modulation from bulk to layered film. *Adv. Mater.* 29:1603157. doi: 10.1002/adma.201603157

Chiang, C.-J., Kimyonok, A., Etherington, M. K., Griffiths, G. C., Jankus, V., Turksoy, F., et al. (2013). Ultrahigh efficiency fluorescent single and bi-layer organic light emitting diodes: the key role of triplet fusion. *Adv. Funct. Mater.* 23, 739–746. doi: 10.1002/adfm.201201750

El-Sayed, M. (1963). Spin—orbit coupling and the radiationless processes in nitrogen heterocyclics. *J. Chem. Phys.* 38, 2834–2838. doi: 10.1063/1.1733610

El-Sayed, M. (1964). Vanishing first-and second-order intramolecular heavy-atom effects on the ($\pi^* \rightarrow$ n) phosphorescence in carbonyls. *J. Chem. Phys.* 41, 2462–2467. doi: 10.1063/1.1726288

Etherington, M. K., Gibson, J., Higginbotham, H. F., Penfold, T. J., and Monkman, A. P. (2016). Revealing the spin-vibronic coupling mechanism of thermally activated delayed fluorescence. *Nat. Commun.* 7:13680. doi: 10.1038/ncomms13680

Frisch, M., Trucks, G., Schlegel, H., Scuseria, G., Robb, M., Cheeseman, J., et al. (2009). Gaussian 09 Revision D. 01. Wallingford, CT: Gaussian Inc.

Gao, Y., Zhang, S., Pan, Y., Yao, L., Liu, H., Guo, Y., et al. (2016). Hybridization and de-hybridization between the locally-excited (LE) state and the charge-transfer (CT) state: a combined experimental and theoretical study. *Phys. Chem. Chem. Phys.* 18, 24176–24184. doi: 10.1039/C6CP02778D

Grabowski, Z. R., Rotkiewicz, K., and Rettig, W. (2003). Structural changes accompanying intramolecular electron transfer: focus on twisted intramolecular charge-transfer states and structures. *Chem. Rev.* 103, 3899–4031. doi: 10.1021/cr940745l

Guo, F., Karl, A., Xue, Q.-F., Tam, K. C., Forberich, K., and Brabec, C. J. (2017). The fabrication of color-tunable organic light-emitting diode displays via solution processing. *Light Sci. Appl.* 6:e17094. doi: 10.1038/lsa.2017.94

Guo, J., Li, X.-L., Nie, H., Luo, W., Gan, S., Hu, S., et al. (2017). Achieving high-performance nondoped OLEDs with extremely small efficiency roll-off by combining aggregation-induced emission and thermally activated delayed fluorescence. *Adv. Funct. Mater.* 27:1606458. doi: 10.1002/adfm.201606458

Jin, J., Zhang, W., Wang, B., Mu, G., Xu, P., Wang, L., et al. (2014). construction of high Tg bipolar host materials with balanced electron–hole mobility based on 1,2,4-thiadiazole for phosphorescent organic light-emitting diodes. *Chem. Mater.* 26, 2388–2395. doi: 10.1021/cm403388s

Krotkus, S., Kasemann, D., Lenk, S., Leo, K., and Reineke, S. (2016). Adjustable white-light emission from a photo-structured micro-OLED array. *Light Sci. Appl.* 5:e16121. doi: 10.1038/lsa.2016.121

Lee, J., Slootsky, M., Lee, K., Zhang, Y., and Forrest, S. R. (2014). An electrophosphorescent organic light emitting concentrator. *Light Sci. Appl.* 3:e181. doi: 10.1038/lsa.2014.62

Li, W., Liu, D., Shen, F., Ma, D., Wang, Z., Feng, T., et al. (2012). A twisting donor-acceptor molecule with an intercrossed excited state for highly efficient, deep-blue electroluminescence. *Adv. Funct. Mater.* 22, 2797–2803. doi: 10.1002/adfm.201200116

Li, W., Pan, Y., Xiao, R., Peng, Q., Zhang, S., Ma, D., et al. (2014a). Employing similar to 100% excitons in OLEDs by utilizing a fluorescent molecule with hybridized local and chargetransfer excited state. *Adv. Funct. Mater.* 24, 1609–1614. doi: 10.1002/adfm.201301750

Li, W., Pan, Y., Yao, L., Liu, H., Zhang, S., Wang, C., et al. (2014b). A hybridized local and charge-transfer excited state for highly efficient fluorescent OLEDs: molecular design, spectral character, and full exciton utilization. *Adv. Opt. Mater.* 2, 892–901. doi: 10.1002/adom.201400154

Liu, H., Bai, Q., Yao, L., Zhang, H., Xu, H., Zhang, S., et al. (2015). Highly efficient near ultraviolet organic light-emitting diode based on a meta-linked donor-acceptor molecule. *Chem. Sci.* 6, 3797–3804. doi: 10.1039/C5SC01131K

Liu, H., Gao, Y., Cao, J., Li, T., Wen, Y., Ge, Y., et al. (2018). Efficient room-temperature phosphorescence based on a pure organic sulfur-containing heterocycle: folding-induced spin-orbit coupling enhancement. *Mater. Chem. Front.* 2, 1853–1858. doi: 10.1039/C8QM00320C

Liu, T., Zhu, L., Gong, S., Zhong, C., Xie, G., Mao, E., et al. (2017a). A red fluorescent emitter with a simultaneous hybrid local and charge transfer excited state and aggregation-induced emission for high-efficiency, low efficiency roll-off OLEDs. *Adv. Opt. Mater.* 5:1700145. doi: 10.1002/adom.201700145

Liu, T., Zhu, L., Zhong, C., Xie, G., Gong, S., Fang, J., et al. (2017b). Naphthothiadiazole-based near-infrared emitter with a photoluminescence quantum yield of 60% in neat film and external quantum efficiencies of up to 3.9% in nondoped OLEDs. *Adv. Funct. Mater.* 27:1606384. doi: 10.1002/adfm.201606384

Luo, Y., and Aziz, H. (2010). Correlation between triplet triplet annihilation and electroluminescence efficiency in doped fluorescent organic light-emitting devices. *Adv. Funct. Mater.* 20, 1285–1293. doi: 10.1002/adfm.200902329

Mao, Z., Yang, Z., Mu, Y., Zhang, Y., Wang, Y. F., Chi, Z., et al. (2015). Linearly tunable emission colors obtained from a fluorescent–phosphorescent dual-emission compound by mechanical stimuli. *Angew. Chem. Int. Ed.* 54, 6270–6273. doi: 10.1002/anie.201500426

Pan, Y., Li, W., Zhang, S., Yao, L., Gu, C., Xu, H., et al. (2014). High yields of singlet excitons in organic electroluminescence through two paths of cold and hot excitons. *Adv. Opt. Mater.* 2, 510–515. doi: 10.1002/adom.201300467

Peng, Q., Niu, Y., Shi, Q., Gao, X., and Shuai, Z. (2013). Correlation function formalism for triplet excited state decay: combined spin–orbit and nonadiabatic couplings. *J. Chem. Theory Comput.* 9, 1132–1143. doi: 10.1021/ct300798t

Peng, Q., Obolda, A., Zhang, M., and Li, F. (2015). Organic light-emitting diodes using a neutral pi radical as emitter: the emission from a doublet. *Angew. Chem. Int. Ed.* 54, 7091–7095. doi: 10.1002/anie.201500242

Peng, Q., Yi, Y., Shuai, Z., and Shao, J. (2007). Toward quantitative prediction of molecular fluorescence quantum efficiency: role of Duschinsky rotation. *J. Am. Chem. Soc.* 129, 9333–9339. doi: 10.1021/ja067946e

Sun, C., Ran, X., Wang, X., Cheng, Z., Wu, Q., Cai, S., et al. (2018). A twisted molecular structure on tuning ultralong organic phosphorescence. *J. Phys. Chem. Lett.* 9, 335–339. doi: 10.1021/acs.jpclett.7b02953

Tang, C. W., and VanSlyke, S. A. (1987). Organic electroluminescent diodes. *Appl. Phys. Lett.* 51, 913–915. doi: 10.1063/1.98799

Tang, X., Li, X.-L., Liu, H., Gao, Y., Shen, Y., Zhang, S., et al. (2018). Efficient near-infrared emission based on donor-acceptor molecular architecture: the role of ancillary acceptor of cyanophenyl. *Dyes Pigments* 149, 430–436. doi: 10.1016/j.dyepig.2017.10.033

Uoyama, H., Goushi, K., Shizu, K., Nomura, H., and Adachi, C. (2012). Highly efficient organic light-emitting diodes from delayed fluorescence. *Nature* 492, 234–238. doi: 10.1038/nature11687

Wang, C., Li, X., Pan, Y., Zhang, S., Yao, L., Bai, Q., et al. (2016). Highly efficient nondoped green organic light-emitting diodes with combination of high photoluminescence and high exciton utilization. *Acs App. Mater. Interfaces* 8, 3041–3049. doi: 10.1021/acsami.5b10129

Wang, C., Li, X.-L., Gao, Y., Wang, L., Zhang, S., Zhao, L., et al. (2017). Efficient near-infrared (NIR) organic light-emitting diodes based on donor-acceptor architecture: an improved emissive state from mixing to hybridization. *Adv. Opt. Mater.* 5:1700441. doi: 10.1002/adom.201700441

Xiang, C., Koo, W., So, F., Sasabe, H., and Kido, J. (2013). A systematic study on efficiency enhancements in phosphorescent green, red and blue microcavity organic light emitting devices. *Light Sci. Appl.* 2:e74. doi: 10.1038/lsa.2013.30

Xu, S., Chen, R., Zheng, C., and Huang, W. (2016). Excited state modulation for organic afterglow: materials and applications. *Adv. Mater.* 28, 9920–9940. doi: 10.1002/adma.201602604

Yao, L., Pan, Y., Tang, X., Bai, Q., Shen, F., Li, F., et al. (2015). Tailoring excited-state properties and electroluminescence performance of donor acceptor molecules through tuning the energy level of the charge-transfer state. *J. Phys. Chem. C* 119, 17800–17808. doi: 10.1021/acs.jpcc.5b03996

Yao, L., Zhang, S., Wang, R., Li, W., Shen, F., Yang, B., et al. (2014). Highly efficient near-infrared organic light-emitting diode based on a butterfly-shaped donor-acceptor chromophore with strong solid-state fluorescence and a large proportion of radiative excitons. *Angew. Chem. Int. Ed.* 53, 2119–2123. doi: 10.1002/anie.201308486

Zhang, D., Duan, L., Zhang, Y., Cai, M., Zhang, D., and Qiu, Y. (2015). Highly efficient hybrid warm white organic light-emitting diodes using a

blue thermally activated delayed fluorescence emitter: exploiting the external heavy-atom effect. *Light Sci. Appl.* 4:e232. doi: 10.1038/lsa.2015.5

Zhang, Q., Kuwabara, H., Potscavage, W. J. Jr., Huang, S., Hatae, Y., Shibata, T., et al. (2014a). Anthraquinone-based intramolecular charge-transfer compounds: computational molecular design, thermally activated delayed fluorescence, and highly efficient red electroluminescence. *J. Am. Chem. Soc.* 136, 18070–18081. doi: 10.1021/ja510144h

Zhang, Q., Li, B., Huang, S., Nomura, H., Tanaka, H., and Adachi, C. (2014b). Efficient blue organic light-emitting diodes employing thermally activated delayed fluorescence. *Nat. Photonics* 8, 326–332. doi: 10.1038/nphoton.2014.12

Zhang, S., Li, W., Yao, L., Pan, Y., Shen, F., Xiao, R., et al. (2013). Enhanced proportion of radiative excitons in non-doped electro-fluorescence generated from an imidazole derivative with an orthogonal donor-acceptor structure. *Chem. Commun.* 49, 11302–11304. doi: 10.1039/c3cc47130f

Zhang, S., Yao, L., Peng, Q., Li, W., Pan, Y., Xiao, R., et al. (2015). Achieving a significantly increased efficiency in nondoped pure blue fluorescent OLED: a quasi-equivalent hybridized excited state. *Adv. Funct. Mater.* 25, 1755–1762. doi: 10.1002/adfm.201404260

Zhao, Y., and Truhlar, D. G. (2008). The M06 suite of density functionals for main group thermochemistry, thermochemical kinetics, noncovalent interactions, excited states, and transition elements: two new functionals and systematic testing of four M06-class functionals and 12 other functionals. *Theor. Chem. Acc* 120, 215–241. doi: 10.1007/s00214-007-0310-x

Zhou, C., Gong, D., Gao, Y., Liu, H., Li, J., Zhang, S., et al. (2018a). Enhancing the electroluminescent efficiency of acridine-based donor-acceptor materials: quasi-equivalent hybridized local and charge-transfer state. *J. Phys. Chem. C* 122, 18376–18382. doi: 10.1021/acs.jpcc.8b07083

Zhou, C., Zhang, S., Gao, Y., Liu, H., Shan, T., Liang, X., et al. (2018b). Ternary emission of fluorescence and dual phosphorescence at room temperature: a single-molecule white light emitter based on pure organic aza-aromatic material. *Adv. Funct. Mater.* 28:1802407. doi: 10.1002/adfm.201802407

Zhou, C., Zhang, T., Zhang, S., Liu, H., Gao, Y., Su, Q., et al. (2017). Isomerization effect of triphenylamine-acridine derivatives on excited-state modification, photophysical property and electroluminescence performance. *Dyes Pigments* 146, 558–566. doi: 10.1016/j.dyepig.2017.07.056